Biased Brownian motion in narrow channels with asymmetry and anisotropy

Zheng Peng[1,2] and Kiwing To[1,*]
[1]*Institute of Physics, Academia Sinica, Taipei 115*
[2]*School of Physics and Electronics, Central South University, Changsha 410083*
(Received 5 April 2016; published 12 August 2016)

We study Brownian motion of a single millimeter size bead confined in a quasi-two-dimensional horizontal channel with built-in anisotropy and asymmetry. Channel asymmetry is implemented by ratchet walls while anisotropy is introduced using a channel base that is grooved along the channel axis so that a bead can acquire a horizontal impulse perpendicular to the longitudinal direction when it collides with the base. When energy is injected to the channel by vertical vibration, the combination of asymmetric walls and anisotropic base induces an effective force which drives the bead into biased diffusive motion along the channel axis with diffusivity and drift velocity increase with vibration strength. The magnitude of this driving force, which can be measured in experiments on a tilted channel, is found to be consistent with those obtained from dynamic mobility and position probability distribution measurements. These results are explained by a simple collision model that suggests the random kinetic energy transfer between different translational degrees of freedom may be turned into useful work in the presence of asymmetry and anisotropy.

DOI: 10.1103/PhysRevE.94.022902

Effective and selective transport of ions and biomolecules through membrane channels and motors [1–3] is vital to a living cell. The size of these channels is often comparable to that of the matter to be transported, and the channel shape is often asymmetric. It has been suggested that the shape of the channel may play an important role in force generation in the DNA package of bacteriophages [4] and motion of kinesin along microtubules [5]. On the other hand, Brownian motion is inevitable because of the size of the molecules. Therefore, it is worthwhile to study the physics underlying the transport phenomenon of Brownian particles through a channel of comparable width and nontrivial shape, not only to understand vital biological processes but also to improve the design of nano-devices for separation and manipulation of nano-materials [2,6].

The transport behavior of a Brownian particle in a channel with varying cross section has been studied for a long time [7–10]. Clearly if the boundaries of the channel are symmetric and no external force along the channel is present, transport along the channel is impossible. Even if the channel wall is asymmetric, a particle in the channel will perform only unbiased Brownian motion due to thermal fluctuation. Surprisingly we find that the presence of anisotropy, which induces larger random kinetic energy in the transverse direction (with respect to the channel axis) than that in the longitudinal direction, may lead to an effective driving force along the channel. If the transverse degree of freedom, with velocity that follows Gaussian statistics, is considered a thermal bath to the transverse degree of freedom, our finding shows that useful work may be extracted from a thermal bath under suitable symmetry breaking. A simple theory based on collision dynamics of the particle with the channel walls can explain the origin of the driving force, which is related to the position distribution of the particle in the channel.

In this study, the Brownian motion of a single millimeter size bead confined in a vertically vibrated quasi-two-dimensional horizontal channel as shown in Fig. 1(a). The channel is composed of connected cells with asymmetric walls. A channel, which is composed of 12 identical cells arranged in four connected branches fabricated by an automated milling machine (Roland MDX-540) on a single piece of black acrylic plate, is mounted on an electromagnetic shaker (Vibration Source Technology VS-300) that oscillates the channel sinusoidally in the vertical direction. A 6 mm diameter plastic bead of mass $m = 0.11$ g is placed in the channel, and a transparent acrylic plate is used as the top cover to the channel. Each cell is bounded by a wall that follows equation

$$y_u(x) = \begin{cases} a + bx & 0 \leqslant x < x_m \\ a_1 + b_1 x & x_m \leqslant x < L \end{cases} \tag{1}$$

and another wall $y_d(x) = -y_u(x)$. Here x is the position along the longitudinal direction as shown in Fig. 1(b). The height of the walls is 15 mm, the length of a cell is $L = 56$ mm, the half-width of the bottleneck is $a = 5.6$ mm, $b = \tan(\pi/6)$, $a_1 = a + L/b$, and $b_1 = -1/b$. The length of the wall W_1 between $x = 0$ and $x = x_m$ is $L_1 = 48.5$ mm and that of the wall W_2 between $x = x_m$ and $x = L$ is $L_2 = 28$ mm. The width w of the cell becomes $y_u - y_d = 2y_u$, and the widest location in the cell is at $x_m = \frac{3}{4}L = 42$ mm. Semicircular ridges of 6 mm diameter and spaced 9 mm apart are machined at the base of the cells as shown in Fig. 1(c). These ridges are parallel to the longitudinal direction (x axis) to provide anisotropy for the cell so that a bead can acquire a horizontal impulse perpendicular to the longitudinal direction when it hits the base.

We label the cells by the branch number and their position in the branch as shown in Fig. 1(d). The electromagnetic shaker drives the channel in vertical sinusoidal oscillation with frequency $f = 30, 40, \ldots, 90$ Hz and amplitude $A = 1, 2$ mm. A fast camera (Prosilica GE680) is used to capture images from above. It is programed to take 10 frames at 100 frames per second within each 0.2 s for at least 2 h. In this way, we capture image sequences of two different time scales: 0.01 and 0.2 s. The position of the bead is located in each frame using

*ericto@gate.sinica.edu.tw

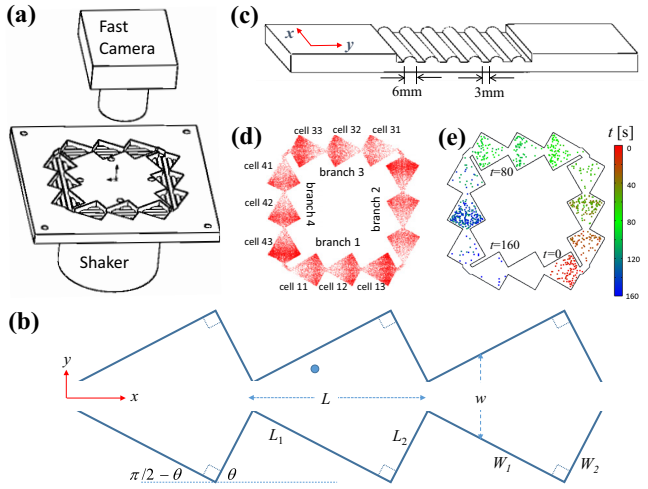

FIG. 1. (a) Schematic diagram of experimental setup. (b) Schematic of a branch. (c) The shape and dimension of the grooves on the channel base. (d) Position distribution of the beads recorded at $f = 60$ Hz and $A = 1$ mm. (e) Positions of bead along the channel in 160 s duration every 0.2 s. The vertical color bar at the right shows the time in seconds.

standard imaging software [11]. The fast image sequences are used for velocity measurements, while the slow image sequences are used for measuring the position distribution, the long time diffusion, and the drift velocity of the bead.

Figure 1(d) is a typical plot of the bead positions. One can see that the position distribution in each of the four branches is qualitatively the same while the distribution within one cell is nonuniform. We calculate the position probability density in a branch $P_b(x)$, which is defined as the ratio $\frac{n(x,\Delta x)}{n_b \Delta x}$ where n_b and $n(x,\Delta x)$ are, respectively, the total number of points in the branch and the number of points in the interval $(x, x+\Delta x)$. Figure 2 shows that $P_b(x)$ for the four branches are indeed the same within experimental uncertainty, as expected from

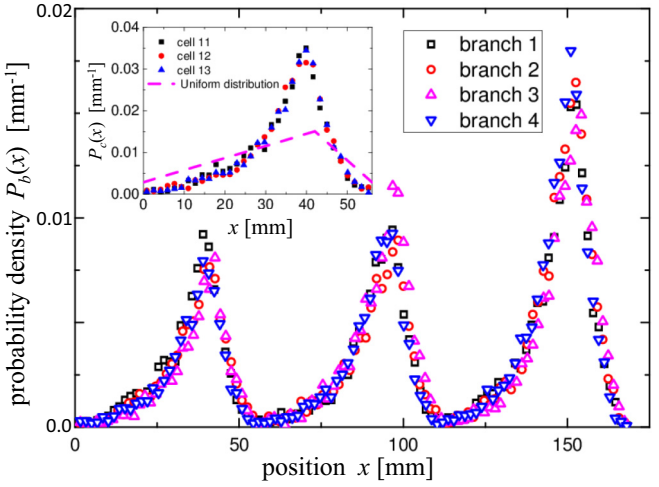

FIG. 2. Probability density of the bead $P_b(x)$ in the four branches at $A = 1$ mm, $f = 60$ Hz. Inset shows the probability density $P_c(x)$ of the cells in branch 1. The dash line in the inset is the expected $P_c(x)$ if the bead positions are uniformly distributed within the cell.

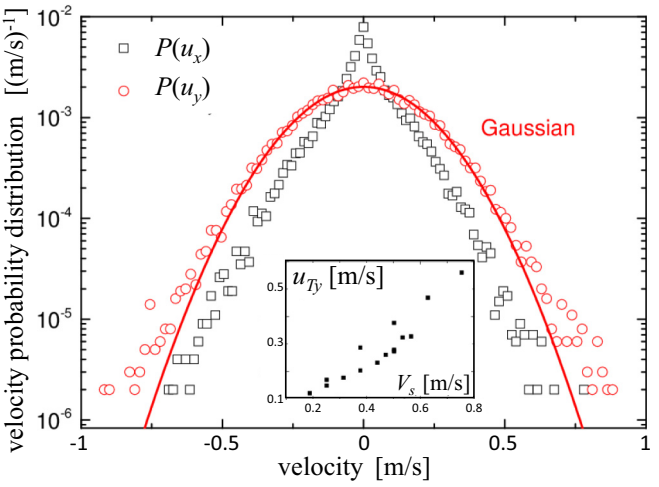

FIG. 3. Velocity distribution of u_x and u_y at vibration condition $A = 1$ mm, $f = 60$ Hz. The solid line is a Gaussian fit for $P(u_y)$. Inset shows that thermal speed u_{T_y} increases with increasing vibration strength V_s.

symmetry argument. However, the number of points in each cell n_c within the same branch are different. Nevertheless the position probability density in a cell $P_c(x) = \frac{n(x,\Delta x)}{n_c \Delta x}$ is the same for each cell as shown in the inset of Fig. 2. Hence, the robust and nontrivial distribution $P_c(x)$ depends only on the asymmetric cell boundaries and the anisotropy induced by the ridges on the base of the cell. If the bead is uniformly distributed in the cell, one would expect $P_c(x)$ to be a piecewise linear function as indicated by the dashed lines in the inset.

Using the fast image sequences we obtain the longitudinal velocity u_x and the transverse velocity u_y of the beads. Figure 3 shows the velocity distributions $P(u_x)$ and $P(u_y)$ measured at $A = 1$ mm and $f = 60$ Hz. We find that $P(u_y)$ follows a Gaussian distribution. This suggests that the transverse degree of freedom has reached thermal equilibrium and hence can be characterized by a thermal speed $u_{T_y} = \sqrt{\langle u_y^2 \rangle}$. The inset of Fig. 3 shows that u_{T_y} increases with increasing vibration strength (denoted by the maximum speed of the channel $V_s = 2\pi A f$ in the vertical direction) as expected.

Using an image sequence of every 0.2 s, we locate the position of the bead and calculate the displacement $x(t)$ along the longitudinal direction. An average movement of the bead in the counterclockwise direction is apparent from the position records shown in Fig. 1(e). Although $x(t)$ fluctuates at a small time interval, it increases linearly with t over a long time [see Fig. 4(a)], and the drift velocity v_d is found to increase linearly with the thermal speed u_{T_y} as shown in Fig. 4(b). On the other hand, the fluctuation $\delta x(t)$ has a mean-squared-displacement $MSD \equiv \langle [\delta x(t+\Delta t) - \delta x(t)]^2 \rangle$ that is proportional to the time lag Δt as shown in Fig. 4(c). Hence, the bead performs biased diffusive motion with a diffusivity D such that $MSD = 2D\Delta t$. Figure 4(d) shows that D is constant at small u_{T_y} and increases linearly with u_{T_y} at large u_{T_y}. The presence of finite drift along the channel suggests the presence of an effective force along the longitudinal direction. To measure this force, we repeat the experiment with both ends of each branch blocked and mount the channel

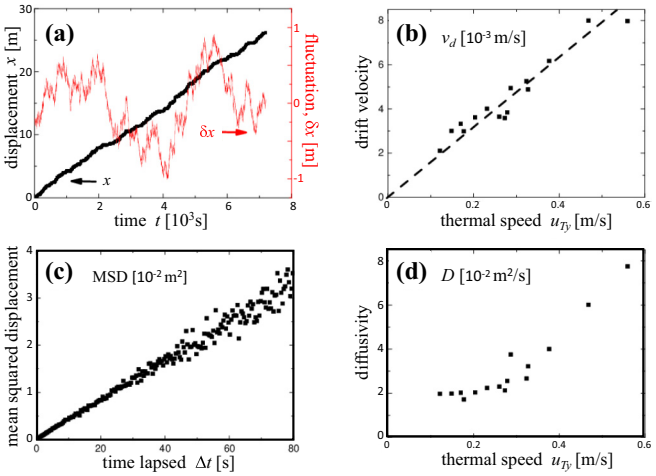

FIG. 4. (a) The time dependent of the displacement x (thick black line) and the fluctuation δx (thin red line). (b) Variation of the drift velocity with thermal speed u_{T_y}. (c) *MSD* of δx. (d) Diffusion constant versus u_{T_y}.

at an angle $\phi = 0.7°, 0.8°, 1.1°, 1.5°$ to the horizontal so that the bead experiences a force $mg\sin\phi$ due to gravity along (against) the longitudinal direction in branch 1 (branch 3). Here $g = 9.81\ \mathrm{m/s^2}$ is the acceleration due to gravity. Figure 5 is a semilog plot of the probability density $P_b(x)$ for different branches at inclined angle $\phi = 1.5°$ with vibration amplitude $A = 1$ mm and frequency $f = 40$ Hz. One can see that the bead spends most of its time in cell 3 of branch 1, whereas the bead spends nearly an equal amount of time in each of the three cells of branch 3. Hence, the net force on the bead along the x direction should vanish in branch 3. So the driving force may be estimated to be $\approx mg\sin 1.5° = 2.56 \times 10^{-5}$ N.

Figure 5 implies that the probability density for a cell $P_c(x)$ depends on inclination. For example, in branch 1 (black squares), $P_c(0)$ is smaller than $P_c(L)$ for cell 12.

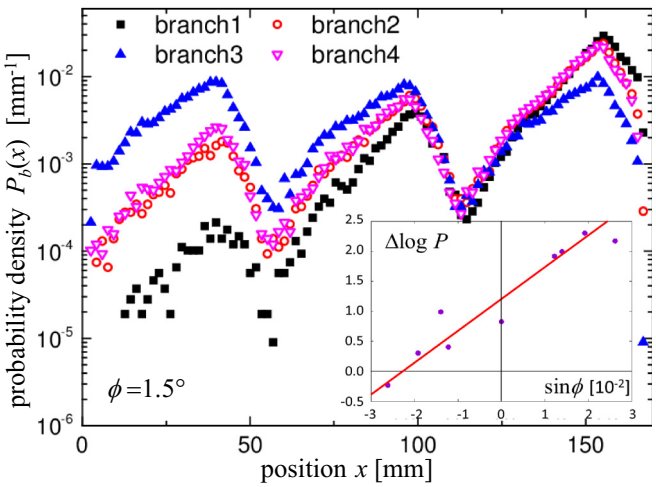

FIG. 5. Reduced probability density $P_b(x)$ in different branches measured at $A = 1$ mm, $f = 40$ Hz, and inclined angle $\phi = 1.5°$. Inset shows that $\Delta\log P$ (defined in text) increases almost linearly with $\sin\phi$; the solid line is a linear fit with horizontal intercept $= -2.27 \times 10^{-2} \pm 14\%$.

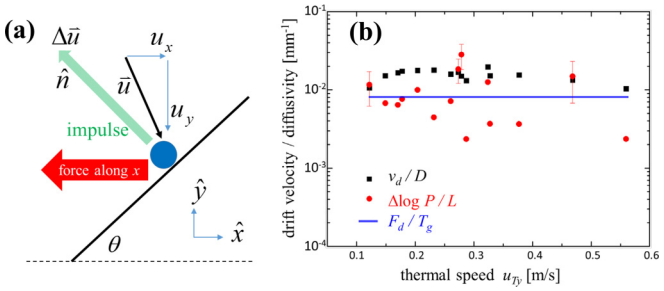

FIG. 6. (a) Schematic diagram of a bead colliding with a wall making an angle θ with the channel axis. (b) Ratio between drift velocity and diffusivity v_d/D versus thermal speed u_{T_y}. Values of $\Delta\log P/L$ are obtained from position density measurements under different vibration conditions, and F_d/T_g is that calculated using Eq. (5).

Interestingly, when the logarithm of the ratio $P_c(L)/P_c(0)$ is plotted against inclination, a linear relation between $\Delta\log P \equiv \log[P_c(L)/P_c(0)] = \log P_c(L) - \log P_c(0)$ versus $\sin\phi$ is revealed as shown in the inset of Fig. 5. Note that the horizontal intercept when multiplied by mg gives the magnitude of the driving force. The driving force thus obtained is $2.46 \times 10^{-5}\ \mathrm{N} \pm 14\%$.

Since the drift velocity vanishes in channels with symmetric walls, i.e., $b = -b_1$ in Eq. (1), a finite drift velocity implies the presence of a driving force originated from the asymmetric walls. Consider a typical collision of the bead to the wall W_2 in a cell as shown in Fig. 6(a). The velocity change after a collision is $\Delta\vec{u} = -\lambda\vec{u}\cdot\hat{n}\hat{n}$ where $\vec{u}$ is the precollision velocity of the bead and $\lambda = (1+\alpha)$ with $\alpha = 0.92$ being the restitution coefficient. As shown in the figure, velocity change in the longitudinal direction is

$$\Delta u_x = -\lambda\sin^2\theta u_x + \lambda\cos\theta\sin\theta u_y. \tag{2}$$

Then the average force experienced by the bead along the channel axis is given by $\nu_2 m\langle\Delta u_x\rangle = -\gamma_2\langle u_x\rangle + \nu_2\kappa\langle u_y\rangle$ where $\gamma_2 = \nu_2 m\lambda\sin^2\theta$, $\kappa = m\lambda\cos\theta\sin\theta$, and ν_2 is the collision frequency, which can be considered as the probability of the bead hitting the wall per unit time. In the situation depicted in Fig. 6(a) with $\theta < \pi/2$, u_y is more probably pointing downward for collision to occur. Hence, we consider only negative values of u_y and replace $\langle u_y\rangle$ by $-\langle|u_y|\rangle$. Using a similar argument, the average force of the bead in the x direction due to collision with W_1 is $\nu_1 m\langle\Delta u_x\rangle = -\gamma_1\langle u_x\rangle + \nu_1\kappa\langle|u_y|\rangle$ where $\gamma_1 = \nu_1 m\lambda\cos^2\theta$. Hence, the total average net force due to collisions with W_1 and W_2 is

$$F_x = -(\gamma_1+\gamma_2)\langle u_x\rangle + (\nu_1-\nu_2)\kappa\langle|u_y|\rangle. \tag{3}$$

Adding the other two walls on the other side, the total force on the bead in the cell is $2F_x$, which can be written as $m\frac{d}{dt}\langle u_x\rangle$. Since $\gamma_{1,2} > 0$, the first term in Eq. (3) is proportional to $-\langle u_x\rangle$. It acts like an effective viscous force (friction) to the beads and hence does not contribute to the drift. It is the second term, $(\nu_1-\nu_2)\kappa\langle|u_y|\rangle$, which is possible to drive the bead along the channel. At steady state when the driving force is balanced by the effective friction, we have $\langle u_x\rangle = \frac{\nu_1-\nu_2}{\gamma_1+\gamma_2}\kappa\langle|u_y|\rangle \propto \langle|u_y|\rangle$. This is consistent with our experimental finding in Fig. 4(b) since $\langle u_x\rangle$ is the drift velocity and $\langle|u_y|\rangle = \sqrt{\frac{2}{\pi}\langle u_y^2\rangle} = \sqrt{\frac{2}{\pi}}u_{T_y}$.

Let the overall collision rate of the bead with all four walls in the cell be ν_o. Then we have $\nu_{1,2} = \frac{\nu_o}{2}\frac{L_{1,2}}{L_1+L_2}$ Here we assume uniform probability density along the walls for simplicity. The overall collision rate ν_o can be approximated by $\langle|u_y|\rangle/\bar{w}$ where $\bar{w}$ is the average half width of the channel. Then the driving force can be expressed as

$$F_d = \frac{m}{\bar{w}}\frac{L_1 - L_2}{L_1 + L_2}\lambda\cos\theta\sin\theta\langle|u_y|\rangle^2. \tag{4}$$

Substituting the values of the parameters ($m = 0.11$ g, $\bar{w} = 17.7$ mm, $L_1 = 48.5$ mm, $L_2 = 28$ mm, $\lambda = 1.92$, $\theta = 60^\circ$, $\langle|u_y|\rangle = 120$ mm/s) in our experiment, we have $F_d = 1.96 \times 10^{-5}$ N, which is the same order of magnitude to that measured in the inclined channel experiment.

Since $\langle|u_y|\rangle^2 = \frac{2}{\pi}u_{T_y}^2$, the above expression for F_d can be rewritten in terms of the granular temperature $T_g \equiv mu_{T_y}^2$ so that

$$\frac{F_d}{T_g} = \frac{2}{\pi\bar{w}}\lambda\cos\theta\sin\theta\frac{L_1 - L_2}{L_1 + L_2}, \tag{5}$$

which depends only on the geometry of the cell. This driving force acts like an effective potential on the bead. When a bead enters the cell of the channel at $x = 0$ and leaves at $x = L$, it experiences a change in the effective potential $U(L) - U(0)$ related to the work done by the driving force such that $F_d L = U(0) - U(L)$. Since the effective potential can be expressed in terms of the position density [12] as $U(x) = -T_g \log P_c(x) + U_o$, we have

$$F_d L = T_g[\log P_c(L) - \log P_c(0)] = T_g\Delta\log P. \tag{6}$$

Here we assume that the effective temperature of the bead in the x direction is comparable to T_g. Then the diffusivity D and the drift velocity v_d are related by the Stokes-Einstein relation: $D = \mu T_g$ where $\mu = v_d/F_d$ is the mobility. So we have $D = T_g v_d/F_d$. Together with Eq. (6), the ratio between the drift velocity and the diffusivity becomes

$$\frac{v_d}{D} = \frac{1}{L}\Delta\log P = \frac{F_d}{T_g}, \tag{7}$$

which connects the dynamic quantities v_d, D, and the steady-state position distribution and the driving force F_d. Here $\Delta\log P$ is defined as $\log P_c(L) - \log P_c(0)$. The above result is confirmed by our experimental data as shown in Fig. 6(b).

To summarize, we observe finite drift of a Brownian bead in a channel with asymmetric walls and anisotropic base. Our observations can be explained quantitatively by a simple collision dynamics theory, which suggests the following picture for the kinetic energy transfer among the different degrees of freedom of the bead. When the bead hits the anisotropic base of the channel, kinetic energy is transferred from the vertical direction to the transverse and longitudinal directions with more energy going to the former. When the bead hits the walls, kinetic energy is transferred from the transverse direction to the longitudinal direction with more energy to the positive than the negative longitudinal direction due to asymmetry of the walls. Hence the bead acquires a finite drift in along the channel axis. In our system, the transverse degree of freedom may be considered a thermal bath at high temperature that transfers heat to the longitudinal degree of freedom at a lower temperature. Then the anisotropy and the asymmetry of the channel act like an engine that generates work, in the form of finite drift velocity, during heat transfer between different degrees of freedom [12]. The efficiency depends on the ratio of the effective temperatures of the transfers and longitudinal degree of freedom. The details are now being studied. On the other hand, the effective net force from collisions with the walls not only drives the bead to drift along the channel axis but also produces a nontrivial position probability density [13], a phenomenon yet to be understood.

The authors would like to thank Prof. C. K. Chan, Prof. Pik-yin Lai, and Prof. Penger Tong for their valuable comments and suggestions. This research is supported by the Ministry of Science and Technology of Taiwan under Grants No. MOST-103-2811-M-001-042 and No. MOST-102-2112-M-001-027-MY2.

[1] P. C. Bressloff and J. M. Newby, Rev. Mod. Phys. **85**, 135 (2013).
[2] P. Hanggi and F. Marchesoni, Rev. Mod. Phys. **81**, 387 (2009).
[3] R. S. Shaw, N. Packard, M. Schroter, and H. L. Swinney, Proc. Natl. Acad. Sci. USA **104**, 9580 (2007).
[4] Pei-Ren Jeng, Kuan-Hua Chen, Gwo-jen Hwang, Chen-Man Tien, Chenhsin Lien, Kiwing To, and Y. C. Chou, Europhys. Lett. **96**, 44005 (2011).
[5] Y. C. Chou, Yi-Feng Hsiao, and Kiwing To, Physica A **433**, 66 (2015).
[6] D. Reguera, A. Luque, P. S. Burada, G. Schmid, J. M. Rubi, and P. Hanggi, Phys. Rev. Lett. **108**, 020604 (2012).
[7] M. H. Jacobs, *Diffusion Processes* (Springer, New York, 1967).
[8] R. Zwanzig, J. Phys. Chem. **96**, 3926 (1992).
[9] D. Reguera and J. M. Rubi, Phys. Rev. E **64**, 061106 (2001).
[10] S. Martens, G. Schmid, L. Schimansky-Geier, and P. Hanggi, Phys. Rev. E **83**, 051135 (2011).
[11] J. C. Crocker and D. G. Grier, J. Colloid Interface Sci. **179**, 298 (1996).
[12] Kiwing To, Phys. Rev. E **89**, 062111 (2014).
[13] Xiao-guang Ma, Pik-Yin Lai, B. J. Ackerson, and Penger Tong, Phys. Rev. E **91**, 042306 (2015).